Check for updates

Li$_4$SiO$_4$ Doped-Li$_7$P$_2$S$_8$I solid electrolytes with high lithium stability synthesised using liquid-phase shaking†

Kazuhiro Hikima, [ID] [a] Ho Jia Ler,[a] Radian Febi Indrawan,[a] Hiroyuki Muto[ab] and Atsunori Matsuda*[a]

In this study, mechanical milling and liquid-phase shaking are used to synthesise 3Li$_2$S·P$_2$S$_5$ LiI·xLi$_4$SiO$_4$ (Li$_7$P$_2$S$_8$I·xLi$_4$SiO$_4$) solid electrolytes. When mechanical milling is used, the electrolyte samples doped with 10 mol% of Li$_4$SiO$_4$ (Li$_7$P$_2$S$_8$I·10Li$_4$SiO$_4$) have the highest ionic conductivity at ~25–130 °C. When liquid-phase shaking is used, they exhibit a relatively high conductivity of 0.85 mS cm^{-1} at ~20 °C, and low activation energy for conduction of 17 kJ mol^{-1}. A cyclic voltammogram shows that there are no redox peaks between −0.3 and +10 V, other than the main peaks near 0 V (*v.s.* Li/Li$^+$), indicating a wide electrochemical window. The galvanostatic cycling test results demonstrate that the Li$_7$P$_2$S$_8$I·10Li$_4$SiO$_4$ has excellent long-term cycling stability in excess of 680 cycles (1370 h), indicating that it is highly compatible with Li. Thus, Li$_7$P$_2$S$_8$I solid electrolytes doped with Li$_4$SiO$_4$ are synthesised using the liquid-phase shaking method for the first time and achieve a high ionic conductivity of 0.85 mS cm^{-1} at 25 °C. This work demonstrates the effects of Li$_4$SiO$_4$ doping, which can be used to improve the ionic conductivity and stability against Li anodes with Li$_7$P$_2$S$_8$I solid electrolytes.

Introduction

All-solid-state lithium-ion batteries contain electrolytes consisting of solid Li$^+$-conducting materials, utilising the discovery of ionic conductors in solid-state ionics. These batteries are of great interest due to their gravimetric and volumetric energy densities, as well as their operational temperature range, safety, low flammability, and resistance to short circuits, in comparison to conventional organic liquid-electrolyte batteries. They represent a new avenue of exploration for electrochemical energy storage, and have great potential for large-scale power generation and storage systems.

In general, Li$^+$-conducting solid electrolytes can be divided into two categories: oxide-type and sulphide-type.[1] Oxide-type solid electrolytes include framework host structures such as perovskites, sodium (Na) super ionic conductors (NASICONs), and garnets, which have been widely reported. They typically have better chemical and electrochemical stability, higher electrochemical oxidation voltages, and greater air stability than sulphide-type solid electrolytes. However, their ionic

conductivities typically plateau at 10^{-3} to 10^{-4} S cm^{-1}, one order of magnitude lower than that of organic liquid electrolytes, because they exhibit high grain-boundary resistance. Another disadvantage is their stiffness, which causes poor interfacial contact and necessitates high-temperature sintering to improve the contacts between the electrodes and electrolytes.

In contrast, sulphide-type solid electrolytes such as Li$_3$PS$_4$,[2] Li$_6$PS$_5$Cl,[3] Li$_7$P$_3$S$_{11}$,[4,5] and Li$_{10}$GeP$_2$S$_{12}$[6] reportedly have superior Li$^+$ conductivity at room temperature. They also have soft crystal lattices, which means they are easy to deform and electrolyte particles can be connected by pressing them together to facilitate ion transport across grain boundaries. However, their application in all-solid-state batteries is limited by their chemical and electrochemical instability, H$_2$S gas emissions, narrow electrochemical windows, and low compatibility with positive/negative electrodes.

Li$_2$S·P$_2$S$_5$·LiI based materials, which have high ionic conductivity and Li stability, are commonly used as solid electrolytes in all-solid-state batteries.[7] Li$_7$P$_2$S$_8$I solid electrolytes have been synthesised using mechanical milling methods, and can achieve a high ionic conductivity of 6.5 mS cm^{-1} (ref. 8) at room temperature (R.T.). Liquid-phase synthesis has also been used, but the ionic conductivity was less than 1.0 mS cm^{-1} at R.T., which is considerably lower than that obtained using mechanical milling,[7–11] although liquid-phase synthesis enables large-scale production of solid electrolytes at low cost. To improve the ionic conductivity, some studies have tried doping Li$_7$P$_2$S$_8$I with other materials. In particular, Li$_7$P$_2$S$_8$I·Li$_3$PO$_4$

[a]Department of Electrical and Electronic Information Engineering, Toyohashi University of Technology, 1-1 Hibarigaoka, Tempaku, Toyohashi, Aichi 441-8580, Japan. E-mail: matsuda@ee.tut.ac.jp

[b]Institute of Liberal Arts and Sciences, Toyohashi University of Technology, 1-1 Hibarigaoka, Tempaku, Toyohashi, Aichi 441-8580, Japan

solid electrolytes have shown relatively high ionic conductivity and lithium stability.[12]

In this study, $3Li_2S \cdot P_2S_5 \cdot LiI \cdot xLi_4SiO_4$ ($Li_7P_2S_8I \cdot xLi_4SiO_4$) solid electrolytes will be synthesised using mechanical milling and liquid-phase shaking methods. The electrochemical properties of the electrolytes will be investigated using cyclic voltammetry (CV) and galvanostatic cycling test. To the authors' knowledge, this has not been reported previously, and the results will contribute to the development of all-solid-state lithium-ion batteries with improved performance.

Experimental details

Solid electrolyte synthesis

The starting materials Li_2S (99.9%, Mitsuwa), P_2S_5 (99%, Merck), and LiI (99.99%, Aldrich) were weighed out with a molar ratio of 3 : 1 : 1 (Li_2S = 0.3827 g, P_2S_5 = 0.6172 g, and LiI = 0.3717 g). The amount of Li_4SiO_4 (99.9%, Toshima, x = 10 mol%, 0.0665 g) used for doping was based on the molar weight of Li_3PS_4 ($3Li_2S \cdot 1P_2S_5$).

For the mechanical milling method, the mixture was manually ground for 15 min, then placed in a 45 mL zirconia (ZrO_2) milling pot with ten 4 mm-diameter zirconia balls, which were used to enhance the kinetics of the reactions between the starting materials. These steps were conducted in an Ar-filled glove box so that the starting materials were not exposed to humidity in the air. Next, the prepared powder was mixed using a planetary ball mill (PULVERISETTE 7; FRITSCH) at 400 rpm for 20 h, which produced the desired solid electrolyte powder. No pre-annealing or post-heat treatments were applied during the preparation.

For the liquid-phase shaking method, the four starting materials were mixed together in a 45 mL centrifuge tube (polypropylene, Labcon) along with 10 mL of EP (ethyl propionate, Aldrich) solvent and approximately 33 g of zirconia balls (ZrO_2 balls, 4 mm). The mixture was then shaken for 3 h at 1500 rpm under a 30 °C in an Ar atmosphere. After shaking, another 6 mL of EP solvent was added to the suspension, which was then dried under low pressure, starting at room temperature, then heated to 70 °C for 1 h, followed by 110 °C for 2 h. The pressure was controlled using a rotary vacuum pump (GHD-031A, ULVAC, Inc). Samples of the resulting electrolyte powder were then heat treated at temperatures of 130–200 °C for 2 h using a tubular furnace (FT-01VAC-30, FULL-TECH). All the processes after the shaking were conducted in a dry Ar-filled glove box.

Characterisation

Crystal structures were assigned to the samples by X-ray diffraction (XRD; Ultima IV, Rigaku). The samples were sealed in specialised holders equipped with a Be window (Rigaku) in an Ar-filled glove box to prevent exposure to humidity. Thermogravimetric differential thermal analysis (TG-DTA; EVO II, Rigaku) was used to evaluate the thermal properties of the solid electrolytes in an Ar-filled glove box. Approximately 8 mg samples of the powders were put in Al pans in an Ar-filled glove box, then heated by 5 °C min^{-1} to 450 °C with Ar gas flow. The morphologies of the samples were examined using a scanning electron microscope (SEM; Hitachi High-Tech, S-4800). A very small amount of each sample was applied and gently distributed on an SEM holder. The SEM images were taken at 5 kV with magnifications of 2.5–25 k (20–2 μm) and they were used to evaluate the microstructures of the samples at different scales.

Electrochemical properties

The temperature dependence of the ionic conductivities of the samples were measured using alternating-current (AC) electrochemical impedance spectroscopy (EIS; SI 1260 Solartron) between 1 MHz and 10 Hz, under an Ar flow atmosphere. A sample weighing approximately 120 mg was uniaxially pressed at 254 MPa at room temperature (approximately 25 °C) to form a pellet 10 mm in diameter. The prepared pellets were placed in a holder made from polyether ether ketone (PEEK) with two blocking electrodes made from stainless steel (SUS). The temperature was increased from room temperature (approximately 25 °C) to 130 °C in 20 °C intervals, the temperature was held at each interval for 1 h before taking the impedance measurement.

CV was conducted using a potentiostat (SI-1287, Solartron). A sample weighing approximately 120 mg was formed into a pellet and uniaxially cold-pressed at 254 MPa at room temperature (approximately 25 °C). Next, a Li-metal sheet 8 mm in diameter and 0.1 mm thick was attached to one side of the prepared pellet, which had a diameter of 10 mm. This was sandwiched between two SUS electrodes. The SUS served as the reference and counter electrodes. The prepared cell (SUS/Li/solid electrolyte/SUS) was measured at a scan rate of 5 mV s^{-1} with a voltage range of −0.3 to +10 V for three cycles.

The galvanostatic cycling test was conducted using Li-metal sheets as the non-blocking electrodes on both sides of the pelletised sample, then sandwiching this between SUS electrodes. The pellet had a diameter of 10 mm and was prepared by uniaxially cold-pressing a 120 mg sample at 254 MPa. The prepared cell (SUS/Li/solid electrolyte/Li/SUS) was electrochemically cycled using a charge–discharge device (BTS-2004H, Nagano) under a dry Ar atmosphere at 30 °C. The current density was fixed at 0.1 mA cm^{-2} and each cycle consisted of 1 h for charging and 1 h for discharging.

Results and discussion

Determination of the doping level

Fig. 1(a) shows the XRD patterns for the ball-milled $Li_7P_2S_8I$ samples doped with 5–30 mol% of Li_4SiO_4. Halo patterns were observed for all the samples, which indicates that the $Li_7P_2S_8$-$I \cdot Li_4SiO_4$ solid electrolytes synthesised using the ball-milling process were amorphous.[13,14] To an extent, two broad peaks were observed at approximately 20° and 29°. However, the x = 30 sample showed sharp peaks that were attributed to one of the starting materials, Li_2S. The presence of residual Li_2S crystals in the x = 30 sample indicates that the sample became Li-rich when it was doped with 30 mol% of Li_4SiO_4.

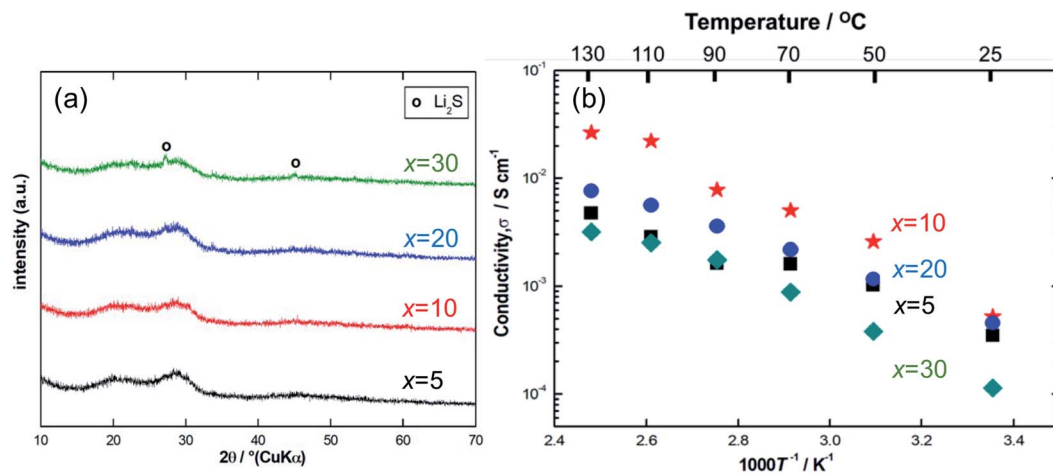Fig. 1 (a) X-ray diffraction patterns, (b) the temperature dependence of ionic conductivity of the ball-milled samples at a Li_4SiO_4-doping composition range of 5 mol% to 30 mol%.

Fig. 1(b) shows the temperature dependence of the ionic conductivity of the $Li_7P_2S_8I \cdot xLi_4SiO_4$ solid electrolytes ($x = 5$, 10, 20, and 30). The $x = 10$ sample had the highest ionic conductivity between room temperature (approximately 25 °C) and 130 °C. At room temperature (approximately 25 °C) the conductivity of the $x = 20$ sample was only slightly lower than that of the $x = 10$ sample, however, at high temperatures the ionic conductivity of the $x = 20$ sample was much weaker, not exceeding 10^{-2} S cm^{-1}, and it was similar to the $x = 30$ sample. Table 1 summarises the ionic conductivity of all the samples ($x = 5$, 10, 20, and 30) at 25 °C. Notably, the ionic conductivity of the $x = 10$ sample increased from 0.52 to 1.4 mS cm^{-1} at 25 °C a substantial increase of one order of magnitude, after the temperature-dependence EIS measurement. In contrast, the $x = 20$ and 30 samples had similar results before and after the EIS measurement, showing no enhancement in their conductivities. This is compatible with the XRD pattern for the $x = 10$ sample after the EIS measurement, which indicates the presence of highly conductive thio-LISICON II analogue phase[11,15–17] as shown in Fig. S2.† The $x = 10$ samples exhibited the highest ionic conductivity, so this doping level was explored further using the liquid-phase shaking method. The TG-DTA curves for the $x = 10$ sample are shown in Fig. S1(a).† The TG curve (blue) showed roughly weight loss of approximately 1% at 300 °C. The DTA curve (red) contained just one exothermic peak at approximately 180 °C, which was caused by the crystallization of $Li_7P_2S_8I$. The DTA curve of the samples after heat treatment at 150 °C contained no peaks (Fig. S1b).†

Liquid phase shaking synthesis

Fig. 2(a) shows the XRD patterns for $Li_7P_2S_8I \cdot xLi_4SiO_4$ ($x = 0$ and 10) solid electrolytes synthesised using the liquid-phase shaking method. It should be noted that no starting material residues, including LiI, were observed in either sample. One peak at 15° was observed in both XRD patterns, this was attributed to the Li_4PS_4I phase, which is poorly conductive of Li$^+$ (0.1 mS cm^{-1} at approximately 25 °C).[15] More peaks attributed to the Li_4PS_4I phase were located between 20° and 40° ($2\theta = 21°$, 27.9°, 29.3°, 29.9°, and 33.4°). In addition, diffraction peaks at $2\theta = 20°$, 25°, and 30° in both samples were attributed to the highly conductive thio-LISICON analogue phase.[11,16,17] Next, the effect of Li_4SiO_4-doping on $Li_7P_2S_8I$ was considered. The peaks attributed to Li_4SiO_4 were not identified and no peak shifts were observed in $Li_7P_2S_8I \cdot 10Li_4SiO_4$. This indicates that Si and O were not incorporated into the $Li_7P_2S_8I$ crystal lattice, and that no solid solution was formed. These XRD patterns have a certain degree of similarity with $Li_7P_2S_8I$ results reported previously.[11,16]

Fig. S3† shows the SEM images for the $Li_7P_2S_8I \cdot xLi_4SiO_4$ ($x = 0$ and 10) solid electrolytes. The primary particle sizes in $Li_7P_2S_8I$ and $Li_7P_2S_8I \cdot 10Li_4SiO_4$ were approximately 5 μm and 2–3 μm, respectively. Although the SEM observations showed no significant differences between the samples, Li_4SiO_4-doping slightly reduced the particle size. Fig. 2(b) shows the ionic conductivity of the $Li_7P_2S_8I \cdot xLi_4SiO_4$ ($x = 0$ and 10) solid electrolytes synthesised using the liquid-phase shaking method.

Table 1 The ionic conductivity of the $Li_7P_2S_8I \cdot xLi_4SiO_4$ ($x = 5$, 10, 20, 30) solid electrolytes at 25 °C before and after Electrochemical Impedance Spectroscopy (EIS) measurements

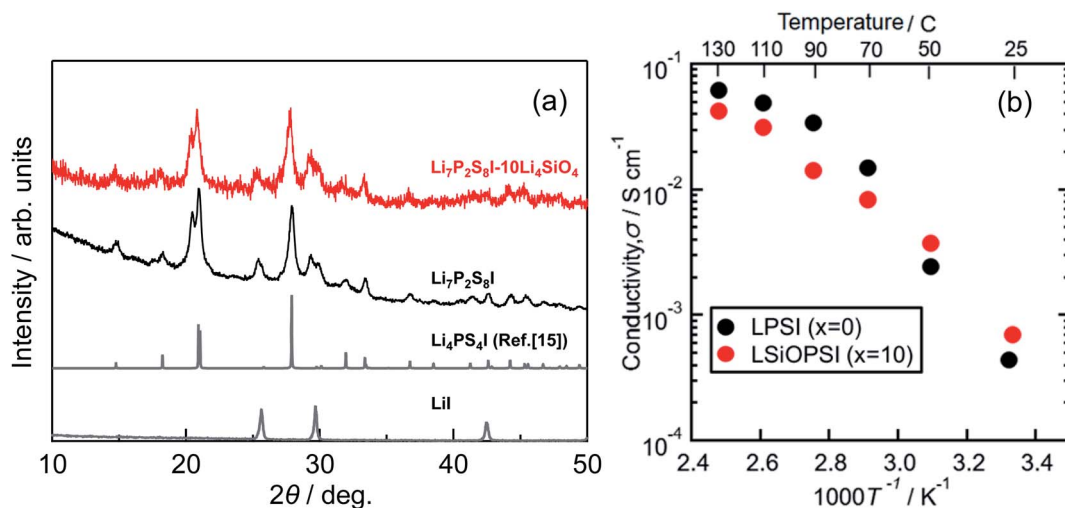| $Li_7P_2S_8I \cdot xLi_4SiO_4$	Ionic conductivity at 25 °C before EIS (mS cm^{-1})	Ionic conductivity at 25 °C after EIS (mS cm^{-1})
$x = 5$	0.35	—
$x = 10$	0.52	1.4
$x = 20$	0.46	0.46
$x = 30$	0.11	0.18

Fig. 2 (a) X-ray diffraction patterns, (b) the temperature dependence of the ionic conductivity of the $Li_7P_2S_8I \cdot xLi_4SiO_4$ ($x = 0$ (LPSI), $x = 10$ (LSiOPSI)) solid electrolytes synthesized by liquid phase shaking method with the heat treatment at 150 °C.
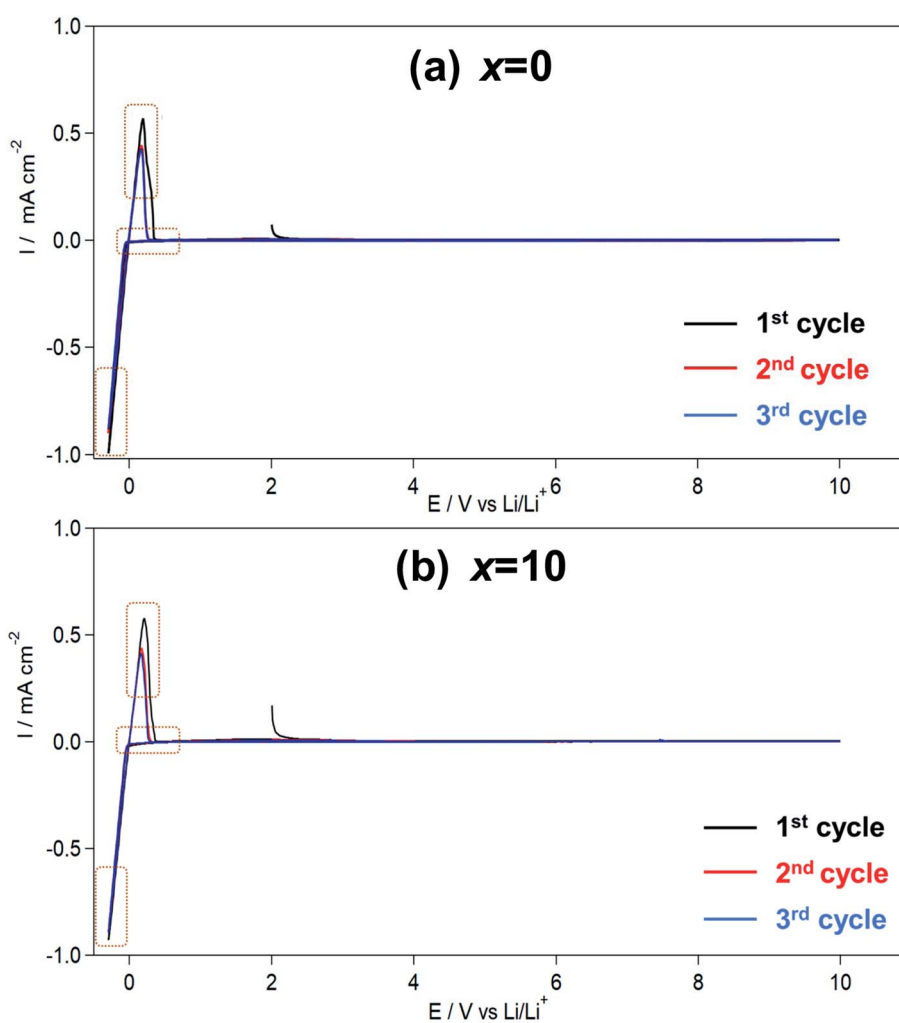

Fig. 3 (a) Cyclic voltammogram of the $Li_7P_2S_8I \cdot xLi_4SiO_4$ ((a) $x = 0$, (b) $x = 10$) solid electrolytes synthesized by liquid phase shaking method with the heat treatment at 150 °C.
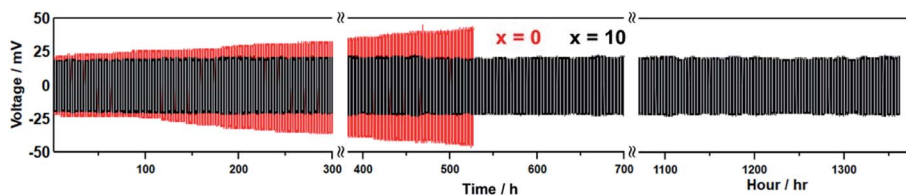
Fig. 4 Galvanostatic cycling test results of the $Li_7P_2S_8I \cdot xLi_4SiO_4$ ($x = 0$, 10) solid electrolytes synthesized by liquid phase shaking method with the heat treatment at 150 °C using Li/solid electrolyte/Li cells.

The room-temperature conductivity of $Li_7P_2S_8I \cdot 10Li_4SiO_4$ was twice that of the undoped sample, increasing from 0.35 to 0.85 mS cm^{-1}. In addition, the activation energy was calculated for the temperature range of 25 °C to 70 °C for $Li_7P_2S_8I$ and Li_7P_2-$S_8I \cdot 10Li_4SiO_4$ respectively, because the temperature dependence of the ionic conductivity of $Li_7P_2S_8I$ was inconsistent with a linear fitting above 90 °C, although this reason is unclear. As a result, the activation energy reduced from 28 to 17 kJ mol^{-1}. As Li_4SiO_4 itself contains lithium ions (4 Li$^+$), the addition of Li_4SiO_4 increased the concentration of Li$^+$ in the $Li_7P_2S_8I$ host material, indicating that an increase in mobile Li$^+$ improved the ionic conductivity. This finding is supported by previous studies.[18,19] In addition, Li_4SiO_4 doping also causes changes in the activation energy. Several earlier studies revealed that Si can reduce energy barriers and Li-site energy for ionic conduction at LGPS-type structures.[19,20] Therefore, it is reasonable to conclude that Li_4SiO_4 is a promising doping candidate for the development of Li$^+$ solid-state conductors with high ionic conductivity at room temperature and a low activation energy.

Effects of Li_4SiO_4 doping

Fig. 3 shows the CV results for the $Li_7P_2S_8I \cdot xLi_4SiO_4$ ($x = 0$ and 10) solid electrolytes synthesised using the liquid-phase shaking method. In both samples, sharp cathodic and anodic peaks were observed at approximately 0.6 V, indicating the occurrence of Li deposition (Li$^+$ + e$^-$ → Li) and dissolution (Li → Li$^+$ + e$^-$). The symmetry of the oxidation–reduction peaks in the CV plots confirmed the good reversibility of Li deposition and dissolution. Moreover, no other large redox peaks were detected between −0.3 and +10 V, demonstrating that $Li_7P_2S_8$-$I \cdot xLi_4SiO_4$ ($x = 0$ and 10) did not decompose in the potential region. In summary, the Li_4SiO_4-doping did not compromise the wide electrochemical windows properties of the solid electrolytes.

Fig. 4 shows the galvanostatic cycling test results for the $Li_7P_2S_8I \cdot xLi_4SiO_4$ ($x = 0$ and 10) solid electrolytes up to 685 cycles (1370 h). A constant current density of 0.1 mA cm^{-2} was applied at room temperature (approximately 25 °C) for 2 h per charge/discharge cycle. The initial voltages of the undoped $Li_7P_2S_8I$ ($x = 0$) and $Li_7P_2S_8I \cdot 10Li_4SiO_4$ solid electrolytes were 23 and 18 mV, respectively. After 50 cycles (100 h), the undoped sample started to reveal signs of voltage increases, and it reached 30 mV by the 130th cycle (160 h), an increase of 23%. In contrast, the doped sample only increased to 20 mV over the same number of cycles. The voltage response of the undoped sample eventually reached 45 mV by the 250th cycle (500 h),

almost double its starting voltage. Over the same number of cycles, the polarization of the doped sample remained stable at 20 mV. After running for more than 250 cycles, the voltage of the undoped solid electrolyte increased by 96%, from 23 to 45 mV, whereas the voltage of the doped solid electrolyte was remarkably consistent increasing from 18 to 20 mV, an increase of just 11%. Therefore, Li_4SiO_4-doping greatly improved the long-term cycling stability of the $Li_7P_2S_8I$ host material with a Li-metal electrode for more than 1300 h of cycling, demonstrating its suitability as a highly Li-compatible and low-resistance interphase. The oxide materials have high Li stability,[1] so this result could reflect the introduction of an oxide ion into $Li_7P_2S_8I$ through the Li_4SiO_4 doping, which is similar to the Li_3PO_4 doped $Li_7P_2S_8I$.

There are several previous reports about Li_4SiO_4 doped Li_2S–SiS_2 type glass solid electrolytes. The Li_4SiO_4 doped Li_2S–SiS_2 type glass solid electrolytes formed the $Si_2OS_6^{6-}$, which consists of one oxygen atom and six sulfur atoms.[21] This $Si_2OS_6^{6-}$ improved the ionic conductivity, because the oxygen atom is introduced as cross-linked oxygen atom with weak trapping of the lithium ion. Therefore, Li_4SiO_4 doped $Li_7P_2S_8I$ solid electrolytes could include the small amount of $Si_2OS_6^{6-}$, although there were no direct evidence. This point is different from our previous report of Li_3PO_4 doped-$Li_7P_2S_8I$.

Conclusion

In this study, $3Li_2S \cdot P_2S_5 \cdot LiI \cdot xLi_4SiO_4$ ($Li_7P_2S_8I \cdot xLi_4SiO_4$) solid electrolytes were synthesised using the mechanical milling and liquid-phase shaking methods. With mechanical milling, 10 mol%-Li_4SiO_4 doping ($Li_7P_2S_8I \cdot 10Li_4SiO_4$) produced the highest ionic conductivity between room temperature (approximately 25 °C) and 130 °C. Therefore, the composition was fixed as the $Li_7P_2S_8I \cdot 10Li_4SiO_4$ for the liquid-phase shaking method. The CV measurement and the galvanostatic cycling test results showed that the electrochemical properties of the $Li_7P_2S_8I$ solid electrolyte were improved by doping with Li_4SiO_4. In particular, the doped electrolyte showed long-term cycling stability against Li-metal over more than 1300 h. This study proved that doping $Li_7P_2S_8I$ solid electrolytes with Li_4SiO_4 has good effects on Li stability.

Author contributions

Conceptualisation, A. M.; methodology, K. H., H. J. L, R. F. I.; software, H. J. L., R. F. I.; validation, K. H., H. J. L., R. F. I.;

formal analysis, H. J. L., R. F. I.; investigation, K. H., H. J. L., R. F. I.; resources, K. H., H. M., A. M.; data curation, K. H., H. J. L., R. F. I.; writing – original draft preparation, K. H., H. J. L.; writing – review and editing, K. H., H. J. L., and A. M.; visualisation, K. H., H. J. L.; supervision, K. H., H. M., A. M.; project administration, K. H., H. M., A. M.; funding acquisition, H. M., A. M.; all authors have read and agreed to the published version of the manuscript.

Conflicts of interest

There are no conflicts to declare.

Acknowledgements

References

1 A. Manthiram, X. Yu and S. Wang, *Nat. Rev. Mater.*, 2017, **2**, 16103.

2 Z. Liu, W. Fu, E. A. Payzant, X. Yu, Z. Wu, N. J. Dudney, J. Kiggans, K. Hong, A. J. Rondinone and C. Liang, *J. Am. Chem. Soc.*, 2013, **135**, 975–978.

3 S. Boulineau, M. Courty, J.-M. Tarascon and V. Viallet, *Solid State Ionics*, 2012, **221**, 1–5.

4 F. Mizuno, A. Hayashi, K. Tadanaga and M. Tatsumisago, *Electrochem. Solid-State Lett.*, 2005, **8**, A603.

5 H. Yamane, M. Shibata, Y. Shimane, T. Junke, Y. Seino, S. Adams, K. Minami, A. Hayashi and M. Tatsumisago, *Solid State Ionics*, 2007, **178**, 1163–1167.

6 N. Kamaya, K. Homma, Y. Yamakawa, M. Hirayama, R. Kanno, M. Yonemura, T. Kamiyama, Y. Kato, S. Hama, K. Kawamoto and A. Mitsui, *Nat. Mater.*, 2011, **10**, 682.

7 E. Rangasamy, Z. Liu, M. Gobet, K. Pilar, G. Sahu, W. Zhou, H. Wu, S. Greenbaum and C. Liang, *J. Am. Chem. Soc.*, 2015, **137**, 1384–1387.

8 X. Feng, P.-H. Chien, S. Patel, J. Zheng, M. Immediato-Scuotto, Y. Xin, I. Hung, Z. Gan and Y.-Y. Hu, *Energy Storage Mater.*, 2019, **22**, 397–401.

9 T. Yamamoto, N. H. H. Phuc, H. Muto and A. Matsuda, *Electron. Mater. Lett.*, 2019, **15**, 409–414.

10 S.-J. Choi, S.-H. Lee, Y.-C. Ha, J.-H. Yu, C.-H. Doh, Y. Lee, J.-W. Park, S.-M. Lee and H.-C. Shin, *J. Electrochem. Soc.*, 2018, **165**, A957–A962.

11 K. Hikima, T. Yamamoto, N. H. H. Phuc, R. Matsuda, H. Muto and A. Matsuda, *Solid State Ionics*, 2020, **354**.

12 R. F. Indrawan, T. Yamamoto, H. H. P. Nguyen, H. Muto and A. Matsuda, *Solid State Ionics*, 2020, **345**.

13 S. Ujiie, T. Inagaki, A. Hayashi and M. Tatsumisago, *Solid State Ionics*, 2014, **263**, 57–61.

14 B. Fan, H. Fu, H. Li, B. Xue, X. Zhang, Z. Luo and H. Ma, *J. Alloys Compd.*, 2018, **740**, 61–67.

15 S. J. Sedlmaier, S. Indris, C. Dietrich, M. Yavuz, C. Dräger, F. von Seggern, H. Sommer and J. Janek, *Chem. Mater.*, 2017, **29**, 1830–1835.

16 S.-J. Choi, S.-H. Choi, A. D. Bui, Y.-J. Lee, S.-M. Lee, H.-C. Shin and Y.-C. Ha, *ACS Appl. Mater. Interfaces*, 2018, **10**, 31404–31412.

17 M. Takahashi, T. Watanabe, K. Yamamoto, K. Ohara, A. Sakuda, T. Kimura, S. Yang, K. Nakanishi, T. Uchiyama, M. Kimura, A. Hayashi, M. Tatsumisago and Y. Uchimoto, *Chem. Mater.*, 2021, **33**, 4907–4914.

18 M. Tatsumisago, K. Yoneda, N. Machida and T. Hinami, *J. Non-Cryst. Solids*, 1987, **95–96**, 857–864.

19 S. P. Ong, Y. Mo, W. D. Richards, L. Miara, H. S. Lee and G. Ceder, *Energy Environ. Sci.*, 2013, **6**, 148–156.

20 A. Kuhn, O. Gerbig, C. Zhu, F. Falkenberg, J. Maier and B. V. Lotsch, *Phys. Chem. Chem. Phys.*, 2014, **16**, 14669–14674.

21 T. Minami, A. Hayashi and M. Tatsumisago, *Solid State Ionics*, 2000, **136–137**, 1015–1023.